

Why is IGR J17091–3624 so faint? Constraints on distance, mass, and spin from ‘phase-resolved’ spectroscopy of the ‘heartbeat’ oscillations

Anjali Rao¹

S. V. Vadawale

Physical Research Laboratory, Ahmedabad-380009, India

ABSTRACT

IGR J17091–3624 is a transient X-ray source and is believed to be a Galactic black hole candidate. Recently, it has received a considerable attention due to the detection of peculiar variability patterns known as ‘heartbeats’, which are quasi-periodic mini-outbursts repeated over timescales ranging between 5 and 70 s. So far, such variability patterns have been observed only in GRS 1915+105 and these are classified as ρ - and ν -variability classes. Here, we present the results of ‘phase-resolved’ spectroscopy of the ‘heartbeat’ oscillations of IGR J17091–3624 using data from simultaneous observations made by RXTE and XMM-Newton. We find that the 0.7–35 keV spectra can be fitted with a ‘canonical’ model for black hole sources consisting of only two components—a multi-temperature disk black body and a power law (or its equivalent). We attempt to constrain the system parameters of the source by simultaneously fitting spectra during different phases of the burst profile while tying the system parameters across the phases. The results indicate that the source is a high inclination binary ($i > 53^\circ$). Further, the observed low flux from the source can be explained only if the black hole spin is very low, along with constraints on the black hole mass ($< 5 M_\odot$) and the distance (> 20 kpc). For higher inclination angles, which is favored by the data, the black hole spin is required to be negative. Thus low or retrograde spin could be the reason for the low luminosity of the source.

Subject headings: accretion, accretion disks — black hole physics — X-rays: binaries — X-rays: individual (IGR J17091-3624)

¹Email: anjali@prl.res.in

1. Introduction

The micro-quasar GRS 1915+105 is an enigmatic black hole binary (BHB) exhibiting enormous variability which have been classified in more than 14 different variability classes (Belloni et al. 2000; Fender & Belloni 2004). It is believed that the extreme variability and rapid state changes observed in GRS 1915+105 are due to a very high accretion rate, which is close to, or at times higher than, the Eddington accretion rate (Done et al. 2004). It is also known for exhibiting large superluminal radio flares and steady radio emission which are always associated with specific X-ray variability classes (Mirabel et al. 1998; Fender et al. 1999; Vadawale et al. 2003). Such an extreme and correlated multi-wavelength variability makes GRS 1915+105 a unique BHB. In this context, IGR J17091–3624, a new X-ray transient source believed to be a BHB, generated considerable interest recently. It was detected by Integral/IBIS in 2003 (Kuulkers et al. 2003). It has exhibited repeated outbursts with periods of two to four years in 1994, 1996, 2001, 2003, 2007, and 2011 (Revnivtsev et al. 2003; Kuulkers et al. 2003; Capitanio et al. 2006, 2009; Krimm et al. 2011; Krimm & Kennea 2011). The recent 2011 outburst of IGR J17091–3624 was unusually long and the source was found to be active even after one year (Altamirano et al. 2012). During this outburst, IGR J17091–3624 revealed its highly variable nature and showed variability patterns so far observed only in GRS 1915+105. The most prominent of these patterns was the ‘heartbeat’ pattern, similar to the ρ -class in GRS 1915+105. Altamirano et al. (2011) documented the first six months of RXTE observations and showed that not only ρ -class but many other variability patterns similar to ν -, α -, λ -, β -, μ -, and χ - classes have been observed during this outburst of IGR J17091–3624. Altamirano & Belloni (2012) also detected a high frequency quasi-periodic oscillation (HFQPO) in this source with a frequency of 66 Hz, which is almost identical to the frequency of HFQPO in GRS 1915+105. Despite striking morphological similarities, the most perplexing difference between the two sources lies in their observed intensities. While GRS 1915+105 is one of the brightest X-ray sources with a typical brightness of $\sim 0.5 - 2$ Crab, IGR J17091–3624 is about 20 times fainter. In the present scenario, mass, distance, and inclination for this source are rather poorly constrained, with reports so far suggesting a mass range of $< 3 M_{\odot}$ (Altamirano et al. 2011) to $\sim 15 M_{\odot}$ (Altamirano & Belloni 2012) and a distance range of ~ 11 kpc (Rodriguez et al. 2011) to ~ 20 kpc (Pahari et al. 2011). Nevertheless, the apparent faintness of IGR J17091–3624 is difficult to explain even after assuming the smallest possible mass of $3 M_{\odot}$ for a black hole (Fryer & Kalogera 2001) and the largest possible distance of ~ 25 kpc for a Galactic source. Here, we attempt to investigate the possible reasons for this apparent faintness of IGR J17091–3624 by simultaneously fitting spectra at different phases. The main idea is that the system parameters cannot change over the phase of the oscillations. Therefore, a simultaneous fitting of spectra at different phases, with system parameters tied across phases, may put a better constraint

on them. This, along with a proposal that the ‘heartbeats’ can be used as a ‘standard candle’, leads to a primary conclusion that the faintness of IGR J17091–3624 is due to its low or negative spin.

2. Observations and Data Analysis

We have used data from long simultaneous observations of IGR J17091–3624 made on 2011 March 27 with RXTE (ObsID: 96420-01-05-000, total exposure ~ 21 ks) and XMM-Newton (ObsID: 0677980201, total exposure ~ 39 ks) with net simultaneous exposure of ~ 15 ks. The data reduction for the RXTE/PCA observation was carried out with HEASoft version 6.8 following standard analysis procedure for Good Xenon data. We extracted 1 s light curve from PCU2 data. It showed the typical ν -class oscillations with periods ranging from 30 to 50 s (Figure 1). It contained a total of 385 bursts. We carried out ‘phase-resolved’ spectroscopy for these bursts in the energy range of 3.0–35.0 keV for RXTE/PCA and 0.7–12.0 keV for XMM/PN data as described below. The peak time for each burst was identified in a semiautomatic manner using an IDL script and the peak-to-peak interval between consecutive bursts was divided into 64 phases of equal length. The start and stop times of each phase, recorded in RXTE mission time for 385 bursts, were used for extracting spectra for each phase. Total counts for all 64 spectra and their corresponding exposure times were then used to generate the ‘phase-folded’ light curve (Figure 2). The 64 phase bins were grouped into five phases as shown in Figure 2 and the spectra extracted for these five phases were used for simultaneous spectral fitting. The grouping was carried out mainly by the visual inspection of the folded RXTE/PCA lightcurve. The XMM observation was carried out in the *fast timing* mode of EPIC-MOS and the *burst* mode of EPIC-PN and we followed the standard analysis procedures for these modes using *SAS v11.0.0* and the latest calibration files. We used data from XMM-PN only because MOS2 data could not be checked for possible pileup (generation of pattern plot always resulted in error) whereas MOS1 data are not useful in timing mode because of a dead pixel in the CCD. For PN data, the observed and the expected pattern behavior differed below 0.7 keV and hence the energy range for rest of the analysis was restricted to 0.7–12.0 keV. Start and stop times of the 64 phases of all bursts from RXTE mission were converted into XMM mission time using the *xTime* tool, available at HEASARC, which were used to build gti files using SAS task *gtibuild*. These gti files were used for extracting the 64 phase spectra using the task *evselect*. The ‘phase-folded’ light curve was generated using the total counts and the exposure times, as described earlier. The subtle features were averaged out as a consequence of the quasi-periodicity and co-adding, but the overall profile of the ‘phase-folded’ light curve followed a typical burst cycle. Further, it was seen that the oscillations were more pronounced in the XMM

light curve indicating that the accretion disk radiation was primarily participating in the oscillations and not the Comptonized emission from the corona which dominates at higher energies. Source spectra from the five grouped phases were extracted using RAWX columns between 32 and 42 for single and double pixel events ($\text{pattern} \leq 4$). SAS tools *rmfgen* and *arfgen* were used to generate redistribution matrices and ancillary files, respectively, and the same files were used for the spectra of all phases. The background spectrum was extracted from RAWX columns between 5 and 7 after confirming that the region was not contaminated significantly with source photons in the selected energy range. A single background spectrum was used for the five phases. All spectra were rebinned using *sastask specgroup* to have a minimum of 25 counts per channel.

2.1. Simultaneous spectral fitting

Once we extracted the spectra for the five phases for both PCA and PN, the 10 spectra were fitted simultaneously with various parameters tied as follows. The 10 spectra were loaded into XSPEC as 10 data groups. For a given phase, all parameters for PCA and PN spectra were tied together except the normalization constant which was frozen at 1.0 for PN whereas for PCA it was kept free but tied across the five phases. For a particular spectral model, we tied all parameters representing system property, such as mass, distance, inclination, spin or combination of these, across the five phases. The parameters describing the accretion process such as inner disk temperature or accretion rate, inner disk radius, were fitted independently for each phase.

3. Results and Discussion

Wide-band X-ray spectrum of a black hole binary generally consists of two dominant components: a multi-color disk and a high-energy tail arising from Compton scattering in an optically thin region surrounding the disk. We used DISKPN (Gierliński et al. 1999) as a simplified disk model, primarily because its parameters are cleanly separated in accretion-process-dependent parameters (disk temperature and inner disk radius) and system parameters (normalization). For a general relativistic description of the multi-temperature disk spectrum, we used KERRBB (Li et al. 2005), which is widely used for its accurate modeling of disk spectrum and to investigate black hole spin. The high-energy tail of the spectrum is typically modeled as POWERLAW to approximate the Comptonized component. However, Steiner et al. (2009b) proposed a more physical model SIMPL to empirically describe the Comptonized component. Here, we have used SIMPL along with one of the two disk models

(DISKPN and KERRBB) to fit the spectra in the five phases simultaneously, as described below.

3.1. Model: DISKPN

For the first part of the analysis, we fitted RXTE-PCA and XMM-PN spectra for the five phases simultaneously with `CONST*PHABS*(SIMPL \otimes DISKPN)`. The parameter `CONST` was used to account for possible calibration uncertainties between the two instruments. Normalizations of `DISKPN` were tied across the five phases, whereas rest of the parameters were allowed to vary independently. Though the interstellar absorption can be considered as a part of system parameters, we allowed it to vary to account for any phase-dependent absorption intrinsic to the source. We, however, found that the N_H values for the five phases were not significantly different and the fitted values of N_H were in agreement with the values reported by Rodriguez et al. (2011) and Krimm et al. (2011). Table 1 provides the results of spectral fits. It can be seen that the inner disk temperature is highest for phase 1 corresponding to the peak of the bursts, implying higher accretion rate as expected. We verified that neither the Fe-line nor the reflection component was required to fit the data. A best fit was obtained with χ^2 value of 1709.0 for 1030 degrees of freedom. However, for the present work, more important is the best-fit value of `DISKPN` normalization, $N_{DPN} = \frac{M^2 \cos(i)}{D^2 f_{col}^4}$, as it can provide some constraints on mass (M), distance (D), and inclination (i). The best fit value of `DISKPN` normalization was found to be $N_{DPN} = 4.0 \times 10^{-4}$. Assuming a minimum mass of $\sim 3 M_\odot$ and a maximum distance of ~ 25 kpc for a Galactic black hole candidate along with a standard value for color correction factor, $f_{col} = 1.7$, the best-fit value of N_{DPN} resulted in a lower limit on inclination angle of 76° . Considering the 90% upper confidence limit of 1.04×10^{-3} for the normalization, the lowest possible inclination angle was $\sim 53^\circ$. This lower limit comes only from simultaneous spectral fitting and it is not dependent on any additional information, and hence it can be considered as fairly robust. Since spectral fitting could not constrain lower limit of N_{DPN} , it was not possible to obtain an upper limit on i with spectral fitting. However, simultaneous spectral analysis with `DISKPN` to model accretion disk spectra suggests that IGR J17091–3624 is a high inclination binary. This is consistent with the finding of Capitanio et al. (2012) and King et al. (2012).

3.2. Model: KERRBB

In the second part, we fitted the spectra using the model `CONS*PHABS*(SIMPL \otimes KERRBB)`. Apart from mass, distance, inclination, and spin as independent fit parameters, `KERRBB` has parameters governing the second-order effects such as ‘spectral hardening factor’, ‘returning

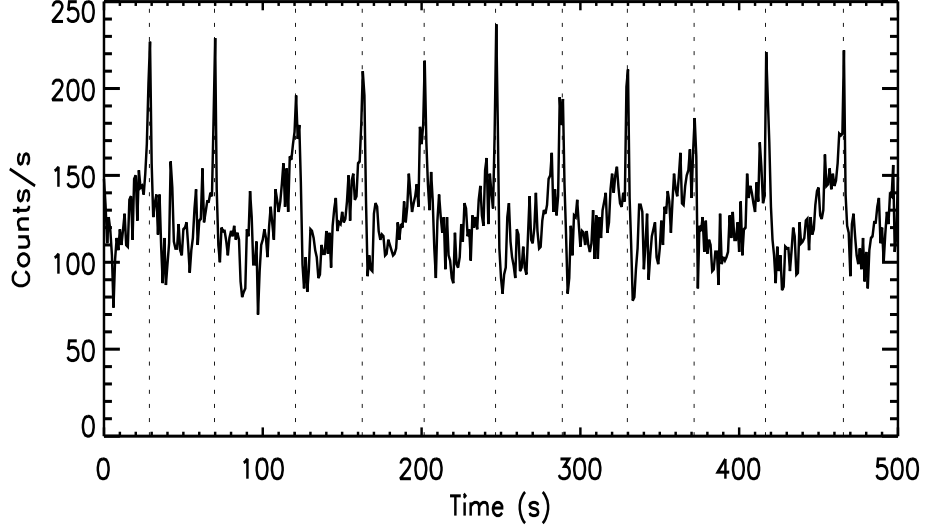


Fig. 1.— RXTE/PCA light curve of IGR J17091-3624 from observation 96420-01-05-000. The light curve was extracted with a bin size of 1 s from PCU2 covering an energy range of 2.0–60.0 keV. The vertical lines show the identified peak times of bursts.

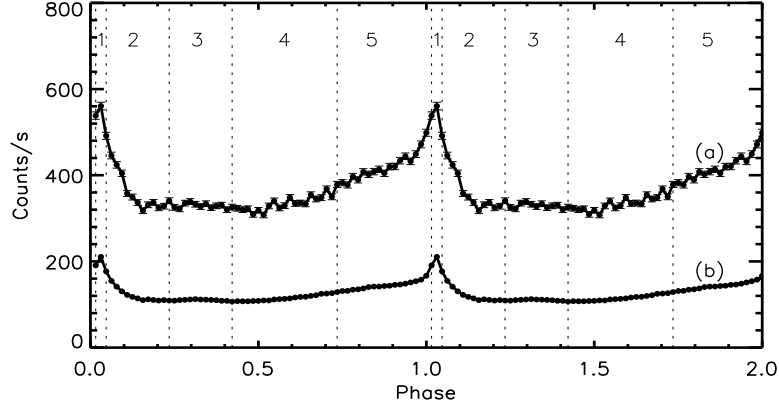


Fig. 2.— Phase-folded light curves from XMM-Newton and RXTE, labeled (a) and (b), respectively. Dotted vertical lines show demarcations for the five phases used for the simultaneous spectral fitting.

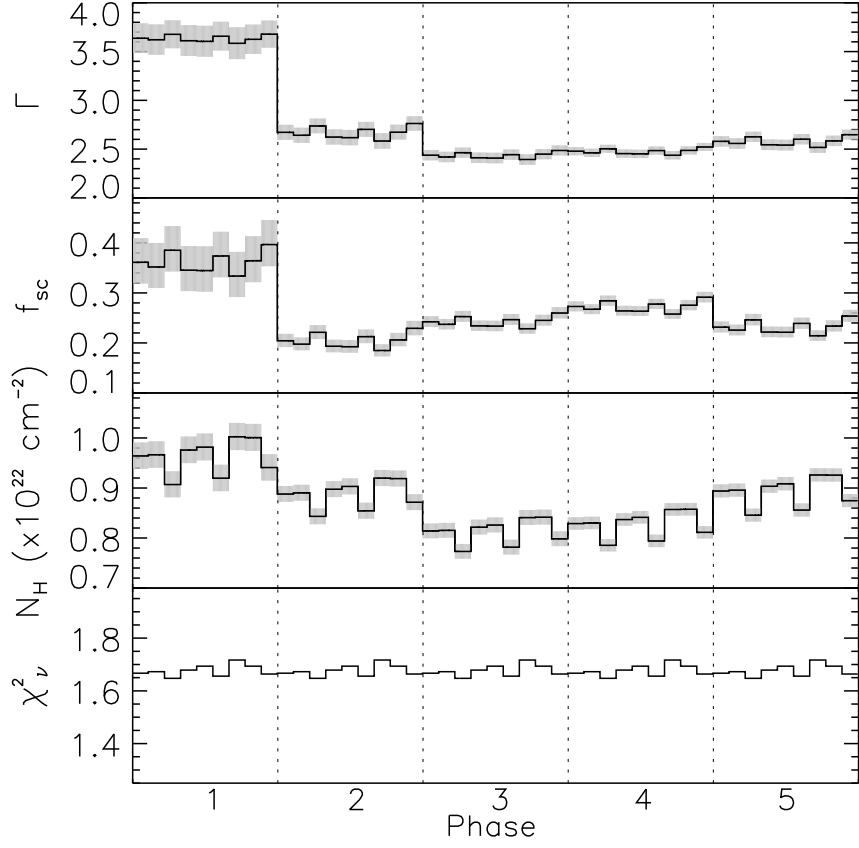


Fig. 3.— Best-fit values for all five phases of Γ , scattering fraction (f_{sc}), N_H , and χ^2_ν for all combinations of D , M , i and a_* . The parameters are more or less similar for any combination of system parameters and hence distinction between them is not made. Error bars (90% confidence) are shown with gray and only a subset of data are shown here.

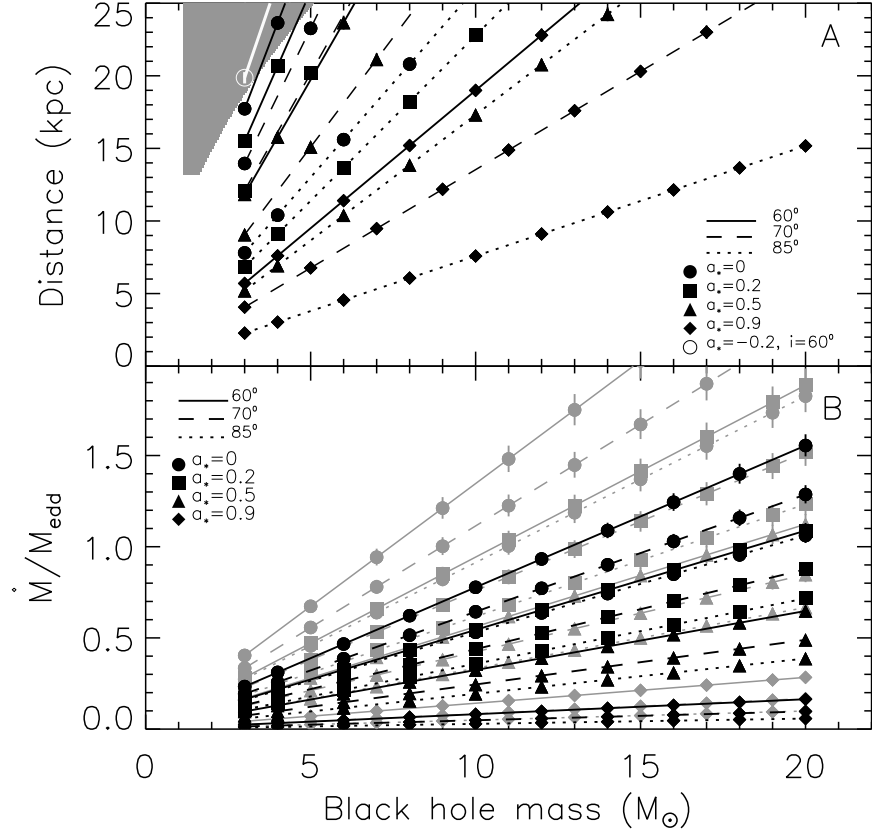


Fig. 4.— Variation of distance (panel (a)) and mass accretion rate (panel (b)) as a function of mass for different inclination angles and spins, as shown in the legend. For the purpose of clarity, symbols are shown for alternate values of mass, and mass accretion rate is shown only for the maximum (gray) and the minimum (black) of the five values. The gray region in the top left corner of panel (a) shows the allowed range for the black hole mass and distance from the luminosity argument.

radiation’ and ‘limb darkening’. We, however, froze these parameters to their default values. Typically KERRBB is used for disk-dominated spectra with luminosity $< 0.3 L_{Edd}$, however, Steiner et al. (2009a) have shown that SIMPL \otimes KERRBB can be used to accurately describe spectra with higher luminosities as well. In this case, we tied all KERRBB parameters except N_H and mass accretion rate across the five phases. Further, the normalization was frozen to 1.0. Since all system parameters cannot be fitted simultaneously, we selected specific values for mass, inclination, and spin and fitted for mass accretion rate and distance. In order to systematically investigate the parameter space, we varied the black hole mass from $3 M_\odot$ to $20 M_\odot$, inclination angle from 50° to 85° , and spin from 0 to 0.9. Results of this analysis have been shown in Figures 3 and 4. Figure 3 shows variation of interstellar absorption, N_H , two parameters of SIMPL – power-law index, Γ and the scattering fraction, f_{sc} , and fit statistic, χ^2_ν for the five phases. Since these parameters are more or less the same for any combination of system parameters (mass, distance, inclination, and spin), these are shown without any distinction. Again it was found that neither the Fe-line nor the reflection component is required for fitting data with the F-test chance improvement probability being $> 88\%$ for all combinations of mass, distance, and inclination. For a combination of mass M , inclination i ($> 50^\circ$), and spin a_* , the fitted values of distance D (top panel) and mass accretion rate \dot{M}_{Edd} (bottom panel) have been shown in Figure 4. Only maximum (phase 1) and minimum (phase 3) mass accretion rates have been shown in Figure 4 for the sake of clarity. Error bars (90% confidence limit) are smaller than the symbols for most of the points in plot. This indicates that the distance and the accretion rate are very well constrained for a given combination of system parameters.

Figure 4 can be used to put some significant limits on the spin of the black hole with some independent constraints on either black hole mass or distance. One such independent constraint comes from the total luminosity argument during ‘heartbeat’ oscillations. Neilsen et al. (2011, 2012) studied such oscillations in GRS 1915+105 and suggested that the radiation pressure instability augmented by the local Eddington limit within inner accretion disk as the origin of such variability pattern. However, this mechanism requires high accretion rate. Neilsen et al. (2011) showed that during the peak of ‘heartbeat’, the bolometric disk luminosity is typically as high as 80%–90 % of the Eddington luminosity. Given the similarity between the variability patterns in GRS 1915+105 and IGR J17091–3624, it is natural to assume a similar mechanism operating in both the sources. In this way, the observed flux during the peak of the ‘heartbeat’ oscillations can be used to estimate the distance for a given mass or in other words ‘heartbeat’ can be used as a standard candle in order to constrain the parameters.

We found the best-fit value of the peak bolometric flux as $4.10 \times 10^{-9} \text{ erg s}^{-1} \text{ cm}^{-2}$. Figure 1 shows that the peak flux in individual bursts is not the same and there is a burst-

to-burst variation in the peak flux values. Therefore, we have assumed the range of peak flux to be $(3.0 - 5.0) \times 10^{-9} \text{ erg s}^{-1} \text{ cm}^{-2}$ and a more conservative range of peak luminosity to be 60%-90% of Eddington luminosity. Thus the obtained possible $M - D$ range is shown as a gray area in the top left corner of Figure 4. It can be seen that the points within this region correspond to inclination angle $< 60^\circ$ and spin < 0.2 . However, the lower limit on inclination was found to be $\sim 76^\circ$ from DISKPN normalization. This presents a tantalizing possibility of black hole spin to be retrograde indicating a black hole spin in opposite direction to the accretion disk. Further, we have found a lower limit of $\sim 53^\circ$ on inclination angle from 90% upper confidence limit of DISKPN normalization. The points corresponding to $i \geq 50^\circ$ require spin to be < 0.2 . Thus we exclude the possibility of high spin and it appears that the main reason for the observed faintness of IGR J17091–3624 is very low (or even negative) spin of the black hole, in contrast to GRS 1915+105, which is known to have a very high spin (McClintock et al. 2006).

It can be seen that even for the exotic type of black hole with mass $< 3 M_\odot$ (Altamirano et al. 2011), this inference on black hole spin remains valid. Further, in order to verify the effect of other frozen parameters of KERRBB, such as returning radiation, limb darkening, and inner boundary stress, we have also enabled all of them (one by one as well as all together) and found that the lines corresponding to a particular combination of spin and inclination angle move away from the shaded region. We verified that the same is valid when POWERLAW is used instead of SIMPL. Thus for any combination of these parameters or model for the high-energy tail, the black hole spin is required to be either very low or negative.

The 66 Hz HFQPO of IGR J17091–3624 detected by Altamirano & Belloni (2012) may also be considered as an independent constraint on black hole mass, if it is assumed to be related to mass. In this case, the black hole mass in IGR J17091–3624 has to be $\sim 15 M_\odot$. For such a high black hole mass, Figure 4(a) does not provide any constraint on the distance, however, both the inclination angle and the spin are required to be $> 70^\circ$ and > 0.7 , respectively. For these high values of inclination angle and spin, Figure 4(b) shows that the required accretion rate is only a small fraction of the Eddington accretion rate. Thus, if we assume that the 66 Hz QPO is related to the black hole mass, the basic accretion process giving rise to the apparent similar variability of GRS 1915+105 and IGR J17091–3624 has to be different. However, it is more likely, as also suggested by Altamirano & Belloni (2012), that the 66 Hz HFQPO is not directly related to the black hole mass. In that case, the previous argument for a low black hole mass based on the apparent flux and similar accretion process between IGR J17091–3624 and GRS 1915+105 holds, and the inference of low or negative spin remains valid. Overall this work indicates that the black hole spin may not play a significant role in generating the observed extreme variability and such a behavior is generated mainly by a high accretion rate.

4. Conclusions

GRS 1915+105 was so far the only BHB exhibiting extreme variability and spectral changes over timescales as short as a few tens of seconds. Observations of similar variability in another BHB IGR J17091–3624 establishes that such extreme variability of GRS 1915+105 is not due to some specific coincidences unique to one particular BHB, but is a more generic phenomenon. Here, we presented results of simultaneous fitting of 0.7–35.0 keV spectra during different phases of the ‘heartbeat’ oscillations in IGR J17091–3624, which indicate that the most likely difference between GRS 1915+105 and IGR J17091–3624 is in the spins of the respective black holes. While the black hole in GRS 1915+105 is known to be rotating with high spin, the black hole in IGR J17091–3624 is found to have a very low spin. In fact, for inclination $\sim 70^\circ$, which is favored by the data, the black hole could very well have a retrograde spin. In this case, IGR J17091–3624 would be the first known astrophysical source having a retrograde spin. Even though theoretically possible, such a scenario would be very challenging to explain from the point of view of evolution of such a system.

This research has made use of data obtained from High Energy Astrophysics Science Archive Research Center (HEASARC), provided by NASA’s Goddard Space Flight Center. We thank A. R. Rao for useful discussions. We also thank the anonymous referee for very useful comments.

REFERENCES

- Altamirano, D., & Belloni, T. 2012, *ApJ*, 747, L4
- Altamirano, D., Wijnands, R., Belloni, T., & Motta, S. 2012, *The Astronomer’s Telegram*, 3913, 1
- Altamirano, D., Belloni, T., Linares, M., et al. 2011, *ApJ*, 742, L17
- Belloni, T., Klein-Wolt, M., Méndez, M., van der Klis, M., & van Paradijs, J. 2000, *A&A*, 355, 271
- Capitanio, F., Del Santo, M., Bozzo, E., et al. 2012, *MNRAS*, 422, 3130
- Capitanio, F., Bazzano, A., Ubertini, P., et al. 2006, *ApJ*, 643, 376

- Capitanio, F., Giroletti, M., Molina, M., et al. 2009, *ApJ*, 690, 1621
- Done, C., Wardziński, G., & Gierliński, M. 2004, *MNRAS*, 349, 393
- Fender, R., & Belloni, T. 2004, *ARA&A*, 42, 317
- Fender, R. P., Garrington, S. T., McKay, D. J., et al. 1999, *MNRAS*, 304, 865
- Fryer, C. L., & Kalogera, V. 2001, *ApJ*, 554, 548
- Gierliński, M., Zdziarski, A. A., Poutanen, J., et al. 1999, *MNRAS*, 309, 496
- King, A. L., Miller, J. M., Raymond, J., et al. 2012, *ApJ*, 746, L20
- Krimm, H. A., & Kennea, J. A. 2011, *The Astronomer’s Telegram*, 3148, 1
- Krimm, H. A., Barthelmy, S. D., Baumgartner, W., et al. 2011, *The Astronomer’s Telegram*, 3144, 1
- Kuulkers, E., Lutovinov, A., Parmar, A., et al. 2003, *The Astronomer’s Telegram*, 149, 1
- Li, L.-X., Zimmerman, E. R., Narayan, R., & McClintock, J. E. 2005, *ApJS*, 157, 335
- McClintock, J. E., Shafee, R., Narayan, R., et al. 2006, *ApJ*, 652, 518
- Mirabel, I. F., Dhawan, V., Chaty, S., et al. 1998, *A&A*, 330, L9
- Neilsen, J., Remillard, R. A., & Lee, J. C. 2011, *ApJ*, 737, 69
- . 2012, *ApJ*, 750, 71
- Pahari, M., Yadav, J., & Bhattacharyya, S. 2011, *ArXiv e-prints*
- Revnivtsev, M., Gilfanov, M., Churazov, E., & Sunyaev, R. 2003, *The Astronomer’s Telegram*, 150, 1
- Rodriguez, J., Corbel, S., Caballero, I., et al. 2011, *A&A*, 533, L4
- Steiner, J. F., McClintock, J. E., Remillard, R. A., Narayan, R., & Gou, L. 2009a, *ApJ*, 701, L83
- Steiner, J. F., Narayan, R., McClintock, J. E., & Ebisawa, K. 2009b, *PASP*, 121, 1279
- Vadawale, S. V., Rao, A. R., Naik, S., et al. 2003, *ApJ*, 597, 1023

Table 1: Parameters Obtained from a Simultaneous Fit to the Spectra of Five Phases with Model **CONS*PHABS*(SIMPL \otimes DISKPN)**

	Phase 1	Phase 2	Phase 3	Phase 4	Phase 5
N_H ($\times 10^{22} \text{cm}^{-2}$)	$0.93^{+0.03}_{-0.03}$	$0.84^{+0.02}_{-0.02}$	$0.81^{+0.01}_{-0.02}$	$0.81^{+0.01}_{-0.01}$	$0.88^{+0.01}_{-0.01}$
T_{max} (keV)	$1.24^{+0.05}_{-0.05}$	$1.11^{+0.01}_{-0.01}$	$1.02^{+0.01}_{-0.01}$	$1.05^{+0.01}_{-0.01}$	$1.11^{+0.01}_{-0.01}$
R_{in} (R_g)	$24.8^{+2.9}_{-2.4}$	$24.9^{+1.2}_{-1.1}$	$28.2^{+1.3}_{-1.2}$	$26.3^{+1.0}_{-0.9}$	$27.3^{+1.0}_{-1.0}$
Γ	$3.57^{+0.25}_{-0.28}$	$2.66^{+0.10}_{-0.10}$	$2.56^{+0.06}_{-0.06}$	$2.52^{+0.04}_{-0.04}$	$2.70^{+0.06}_{-0.06}$
Scattered fraction	$0.47^{+0.02}_{-0.28}$	$0.27^{+0.02}_{-0.02}$	$0.36^{+0.02}_{-0.02}$	$0.37^{+0.01}_{-0.01}$	$0.35^{+0.02}_{-0.02}$
Disk flux ^a	2.10	1.23	1.01	1.06	1.47
Total flux ^a	2.54	1.53	1.42	1.49	1.92
DISKPN norm ^b	$4.0^{+6.4}_{-3.7} \times 10^{-4}$				

a: Unabsorbed flux in units of $\times 10^{-9} \text{erg s}^{-1} \text{cm}^{-2}$ for 2 – 10 keV energy range.

Unabsorbed bolometric disk flux for phase 1 is $4.10 \times 10^{-9} \text{erg s}^{-1} \text{cm}^{-2}$.

(See the text for discussion).

b: Since spectral fitting could not constrain the lower limit of norm, it was calculated from the extreme values of M , D and i .